Int. J. Electrochem. Sci., 15 **(2020)** 1949 – 1963, doi: 10.20964/2020.03.04

International Journal of
ELECTROCHEMICAL
SCIENCE
www.electrochemsci.org

Three-dimensional Hierarchical Structure NiFe Layered Double Hydroxides Nanosheets Based on Carbon Cloth for High Performance Non-Enzymatic Glucose Detection

Dandan Song[1], *Lili Wang*[1,*], *Bing Wang*[1,*], *Jianguo Yu*[1], *Yanting Li*[2], *Yuning Qu*[1],
Cunpeng Duan[2], *Yuying Yang*[1], *Xueli Miao*[2]

[1] State Key Laboratory of Separation Membranes and Membrane Processes, School of Chemistry and Chemical Engineering, Tiangong University, 399 Binshui West Road, Tianjin 300387, P. R. China
[2] School of Environmental Science and Engineering, Tiangong University, Tianjin 300387, China
[*]E-mail: wanglili@tjpu.edu.cn, bingwang@tjpu.edu.cn

Received: 4 October 2019 / *Accepted:* 9 December 2019 / *Published:* 10 February 2020

The construction of non-precious metal nanomaterial with higher sensitivity and better selectivity is very important for glucose detection. In this paper, three-dimensional (3D) hierarchical layered double hydroxide (LDH) nanomaterials (CC@CCH NiFe LDH) are successfully synthesized by simple hydrothermal method. 1D basic cobalt carbonate (CCH) nanorods are preliminarily formed on the carbon cloth (CC), which acts as support, and then 2D NiFe LDH nanosheets are guided to deposit on the surface. Therefore, the hierarchical layered structure was obtained with high surface area and more active sites. The prepared CC@CCH NiFe LDH electrode material possesses excellent electrochemical catalytic oxidation performance. The test results show that the electrode material has high sensitivity (6610 $\mu A \cdot mM^{-1} \cdot cm^{-2}$), wide linear range (0.01-1 mM), fast current response (< 10 s) and low detection limit (3 μM). Furthermore, the sensor material has good selectivity.

Keywords: Carbonized cotton cloth, 3D hierarchical layered structure, NiFe LDH nanosheets, non-enzymatic glucose detection

1. INTRODUCTION

Glucose is important source of body's energy molecule adenosine triphosphate (ATP) [1-3]. However, the high glucose content in the body's physiological fluids can cause various metabolic disorders (such as diabetes). Diabetes is a metabolic disease, which causes kidney, retina and nervous system complications, leading to disability and premature death [1, 4-7]. According to statistics released by the World Health Organization (WHO), the incidence of diabetes has been increasing over the past few decades [1, 8]. Therefore, it is important to develop accurate, reliable and fast glucose determination methods. At present, electrochemical biosensors are widely used in clinical diagnosis, environmental detection, food industry and agricultural [8, 10]. Most of the sensors use glucose oxidase as an enzyme catalyst to ensure the maximum sensitivity and selectivity of the prepared sensing platform [1, 11, 12]. However, the presence of enzymes has following disadvantages. Due to the thermal and chemical instability of the enzyme, the activity of the enzyme is affected by pH, temperature, humidity and toxic chemicals [5, 9, 13-15]. In particular, during the immobilization and stabilization of the enzyme, the determination of glucose in actual samples will be limited to some extent [10, 11, 16]. Therefore, the preparation of enzyme free electrochemical sensors based on direct oxidation on the electrode surface have become a new development trend.

In recent years, based on the unique properties of transition metal nanomaterials, such as high surface area, strong electrocatalytic activity and good chemical stability, people are increasingly interested in developing nanomaterial sensing platforms [1, 7, 17-19]. Among the developed electrode materials, layered double hydroxides (LDHs) are very thin, which is the nanometer scale [18, 20]. Therefore, they can not only expose the surface active sites as much as possible, but also reduce the mass transfer resistance and shorten the ion transport path, thus having better catalytic performance [17, 18, 21-24]. In addition, the morphology of LDHs is crucial to improve electrochemical properties, and it can be carefully adjusted by designing their structures [20, 25]. Therefore, LDHs are favored in the field of non-enzyme electrochemical glucose sensors. In particular, NiFe LDH is considered to be one of the ideal electrocatalytic oxidation materials due to its excellent catalytic activity [18, 20, 26-28]. However, the fabrication of LDHs electrodes faces great difficulties as they tend to form irreversible agglomerates, leading to reduced active site regions; in addition, the poor mechanical stability of powdered LDH nanosheets further inhibits their wide application in the electrochemical field [5, 10, 11, 29-33].

In order to solve above problems, using high conductive carbon material as a support skeleton is an effective and feasible strategy. The three-dimensional (3D) carbon cloth (CC) material can ensure the exposure of the electroactive sites as much as possible. Furthermore, it also can promote efficient charge transfer between the active material and the carbon cloth fibers compared with the conventional dense electrode film [10, 34]. Meanwhile, due to the high flexibility, loose fiber structure and good electrical conductivity of the carbon cloth, glucose is easily diffused at the electrode interface [18]. In addition, the confinement of the 3D carbon skeleton prevents pulverization and aggregation of the LDH nanosheets during electrochemical measurement. Because of its high thermal stability and mechanical stability, excellent electrical conductivity, good corrosion resistance to strong alkaline media, there is no doubt that carbon cloth should be an excellent conductive base [9, 10, 18, 34].

Based on the above considerations, in order to further improve the overall properties of this material, a new 3D hierarchical structure (CC@CCH NiFe LDH) was designed by introducing 1D basic cobalt carbonate (CCH) as a support. The specific preparation is as follows: First, 1D CCH was grown in situ on CC by simple hydrothermal reaction; after that, 2D NiFe LDHs nanosheets were performed on 1D CCH by hydrothermal method. Due to the composite material has rich active site and unique hierarchical structure, which greatly improves its catalytic oxidation ability to glucose. The test results show that under the optimal conditions, CC@CCH NiFe LDH electrode material has high sensitivity (6610 $\mu A \cdot mM^{-1} \cdot cm^{-2}$), fast current response (< 10 s), wide linear range and good selectivity.

2. EXPERIMENTAL

2.1 Chemicals

Cobalt nitrate hexahydrate ($Co(NO_3)_2 \cdot 6H_2O$), urea, iron nitrate nonahydrate ($Fe(NO_3)_3 \cdot 9H_2O$), nickel nitrate hexahydrate ($Ni(NO_3)_2 \cdot 6H_2O$), glucose (Glu), ascorbic acid (AA), cysteine (Cys), potassium chloride (KCl), sodium chloride (NaCl), lactose (Lac), uric acid (UA), fructose (Fru), sucrose (Suc), dopamine (DA) and ethanol are all analytically pure, and they were purchased from Aladdin. The aqueous solutions involved in the experiments were prepared with deionized water.

2.2 Preparation of CC

The carbon cloth (CC) was obtained by carbonizing a commercial cotton cloth under a nitrogen atmosphere. First, the cotton cloth was ultrasonically washed in absolute ethanol and deionized water for 30 min, respectively, and then vacuum dried for 10 h. After that, the dried cotton cloth was carbonized in tube furnace at 800 °C under a nitrogen atmosphere. The heating rate was 5 $°C \cdot min^{-1}$, and the heating time was 90 min [35, 36].

2.3 Preparation of CC@CCH NiFe LDH

First, the prepared CC (1×1 cm^2) was put into a mixture of urea (25 mmol) and $Co(NO_3)_2 \cdot 6H_2O$ (5 mmol), which was thoroughly mixed and transferred to a high pressure reactor at 90 °C for 5 h. The obtained CC@CCH was cleaned by deionized water and vacuum dried at 60 °C for 10 h. Then, the CC@CCH was mixed with $Ni(NO_3)_2 \cdot 6H_2O$ (3 mmol), $Fe(NO_3)_3 \cdot 9H_2O$ (1 mmol) and urea (20 mmol), and it was hydrothermally reacted at 120 °C for 8 h to obtain CC@CCH NiFe LDH. The reaction product was cleaned with deionized water, vacuum dried at 60 °C for 10 h. The possible reactions can be described as follows:

$$CO(NH_2)_2 + 3H_2O \rightarrow 2OH^- + 2NH_4^+ + CO_2 \quad (1)$$

$$Ni^{2+} + Fe^{3+} + OH^- \rightarrow \text{NiFe-LDH} \quad (2)$$

For comparison, CCH and NiFe LDH materials were deposited on CC, and the obtained products were CC@CCH and CC@NiFe LDH, respectively.

2.4 Materials characterization

In this paper, the surface morphology of the samples were characterized by scanning electron microscopy (SEM, Hitachi S4800). The crystal structure was characterized by X-ray diffraction (XRD, Bruker D8 Discover) with a radiation source of Cu-Kα. The elemental composition and valence state of the samples were analyzed by X-ray photoelectron spectroscopy (XPS, K-alpha, Thermo Fisher). The electrochemical performance of the prepared electrode materials were tested in a standard three-electrode system using an electrochemical workstation (CH Instruments, China).

2.5 Electrochemical measurement

The electrochemical properties of the prepared materials were tested using an electrochemical workstation and a typical three-electrode cell. KOH (1 M) was used as the electrolyte, and the working electrode, the counter electrode and the reference electrode were CC@CCH NiFe LDH, platinum plate and Hg/HgO, respectively. Cyclic voltammetry (CV) was used to record a CV curves in the range of -0.2 to 0.7 V. The amperometric i-t curves of glucose detection was recorded at 25 °C under magnetic stirring condition with a control operating potential of 0.60 V.

3. RESULTS AND DISCUSSION

3.1 Characterization of materials structure

The preparation of CC@CCH NiFe LDH electrode material based on CC is shown in Fig. 1. Firstly, high-density CCH nanorods were grown on the surface of CC by hydrothermal method. After that, NiFe LDH nanosheets were deposited on the surface of the CCH nanorods to form a 3D hierarchical layered structure.

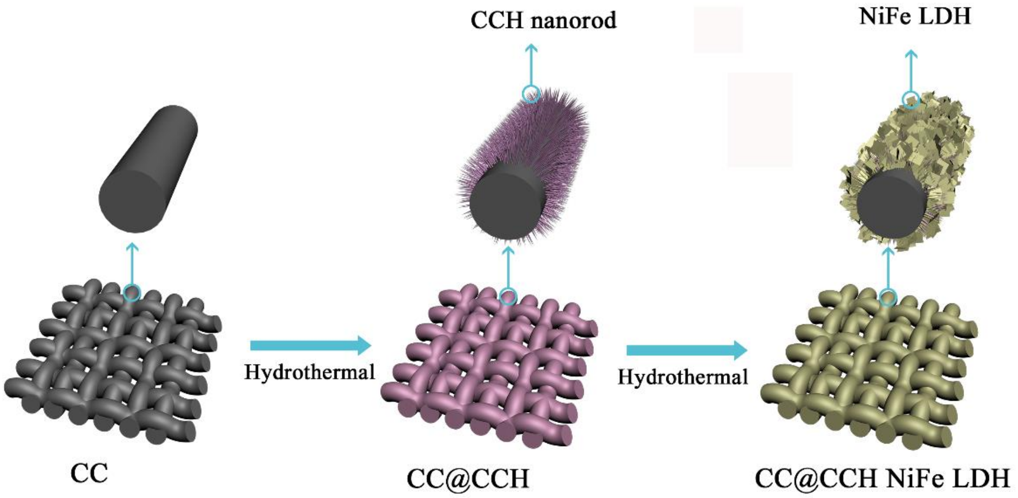

Figure 1. Schematic illustrating of the synthesis process for the CC@CCH NiFe LDH nanosheets on carbon cloth.

Fig. 2 and Fig. 3 show the morphology and microstructure of CC@CCH, CC@CCH NiFe LDH, CC@NiFe LDH. From Fig. 2 (A-B), it can be seen that after hydrothermal treatment, the carbon cloth fiber is covered with a dense layer composed of many nanorods. The obtained CCH nanorods grown on the surface of the CC uniformly, forming an ordered linear array structure, indicating that CC is an ideal conductive substrate. As displayed in Fig. 2 (C-E), the nanoscale CCH nanorods are used as the substrate to guide the directed growth of NiFe LDH. The NiFe LDH forms a regular slice on CCH surface and the lamellar structure is not very dense. These NiFe LDH nanosheets are interpenetrated and intertwined, which not only increases the surface area of the electrode material, but also improves the transfer rate of ions and electrons. Thus, it can improve the electrocatalytic oxidation performance of non-enzymatic glucose. Fig. 3 (A-B) show that NiFe LDH grows directly on CC, forming a coral-like shape with uneven size and less active sites, which is not conducive to the diffusion of electrolyte ions.

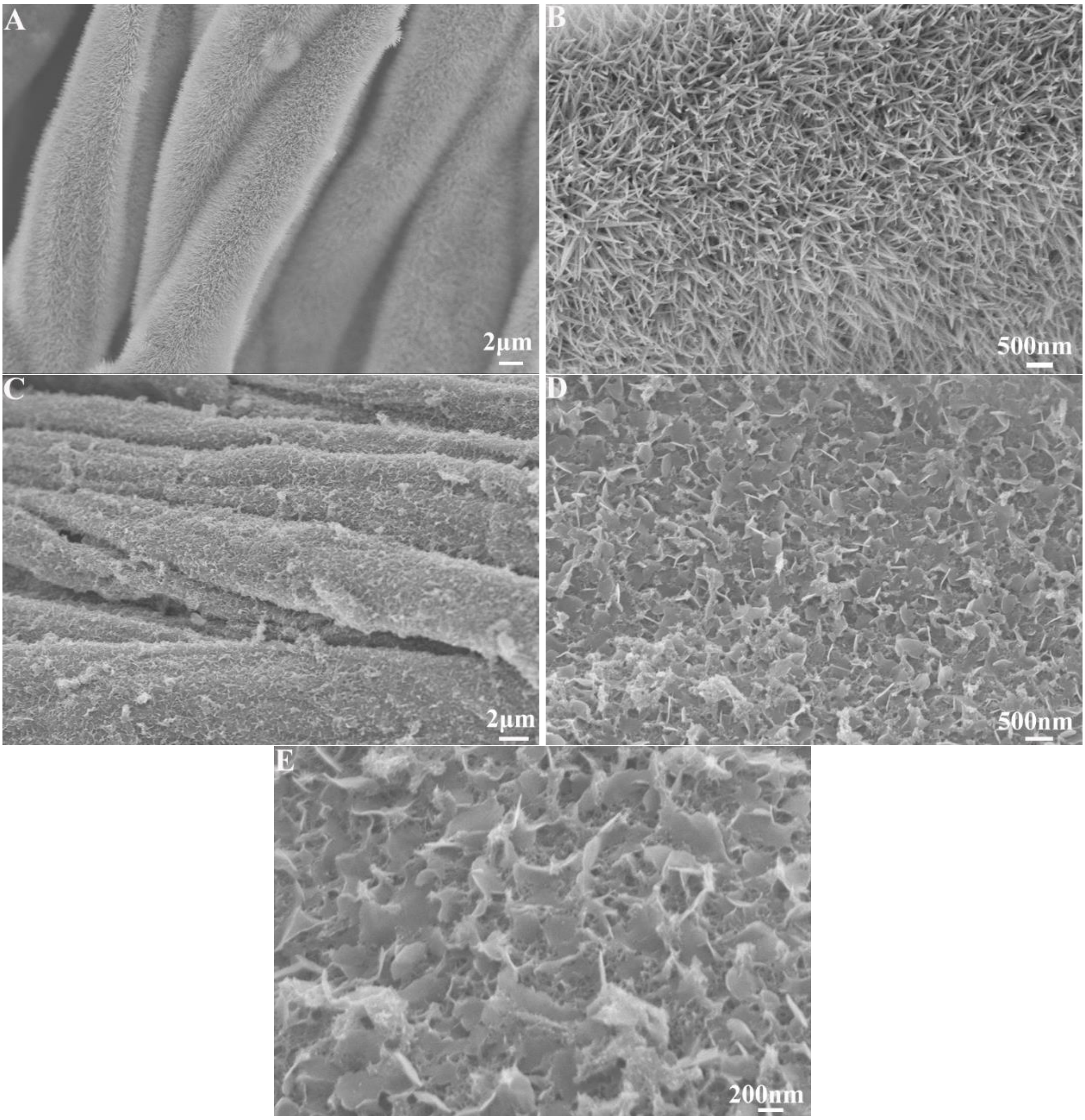

Figure 2. (A-B) SEM images of CC@CCH; (C-E) SEM images of CC@CCH NiFe LDH at different magnification.

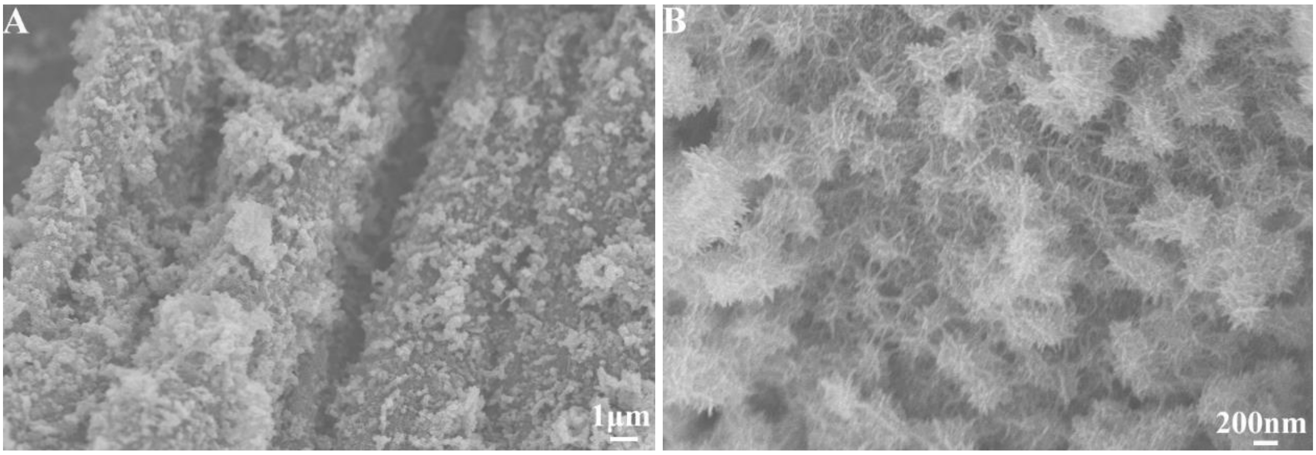

Figure 3. (A-B) SEM images of CC@NiFe LDH at different magnification.

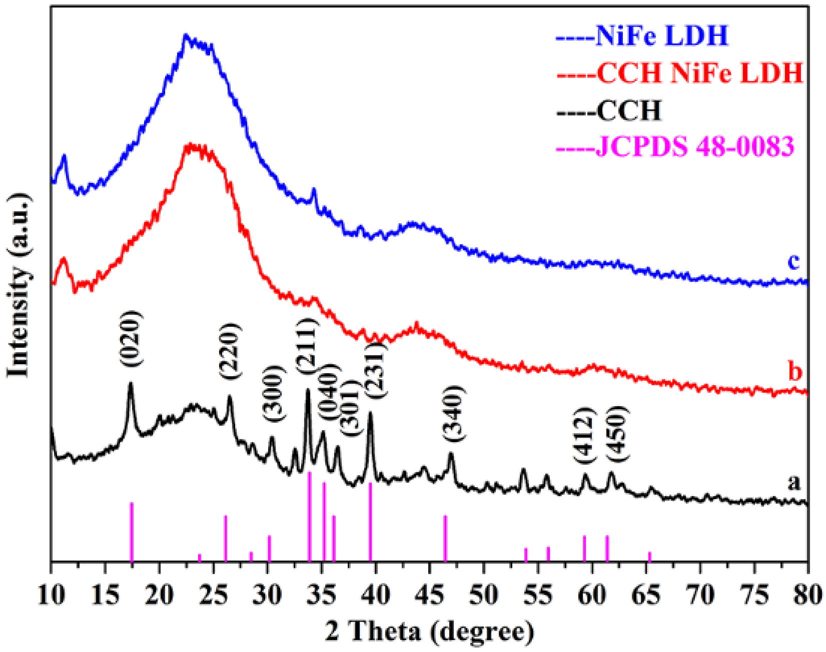

Figure 4. XRD spectra of CC@CCH, CC@CCH NiFe LDH, CC@NiFe LDH.

The crystal structure of the materials were analyzed by X-ray diffraction (XRD), as Fig. 4 shown. The XRD spectrum shown by curve (a) has diffraction peaks at 2θ of 17.26°, 26.38°, 30.35°, 33.62°, 35.14°, 36.37°, 39.43°, 46.85°, 59.32°, and 61.67°, respectively. These diffraction peaks correspond to the (020), (220), (300), (211), (040), (301), (231), (340), (412) and (450) reflection planes, confirming that they are consistent with the structure of CCH nanorods (JCPDS 48-0083) [37, 38]. For CC@CCH NiFe LDH, some new low-intensity diffraction peaks appear at 11.26°, 22.74°, 34.23°, 38.85°, 59.78°, 60.98° as shown by curve (b), which can be well indexed to (003), (006), (012), (015), (110) and (113) plane reflections of hydrotalcite-like LDH phase, indicating the synthesis of NiFe LDH [25, 28, 39]. Furthermore, no other diffraction peaks of Ni and Fe oxides appeared, illustrating that the prepared electrode material is of higher purity. By comparing curves (b) and (c), it can be observed that the diffraction peaks of curve (c) is stronger than that of curve (b). This is because the presence of CCH weakens the diffraction peak of NiFe LDH when CCH is used as the substrate.

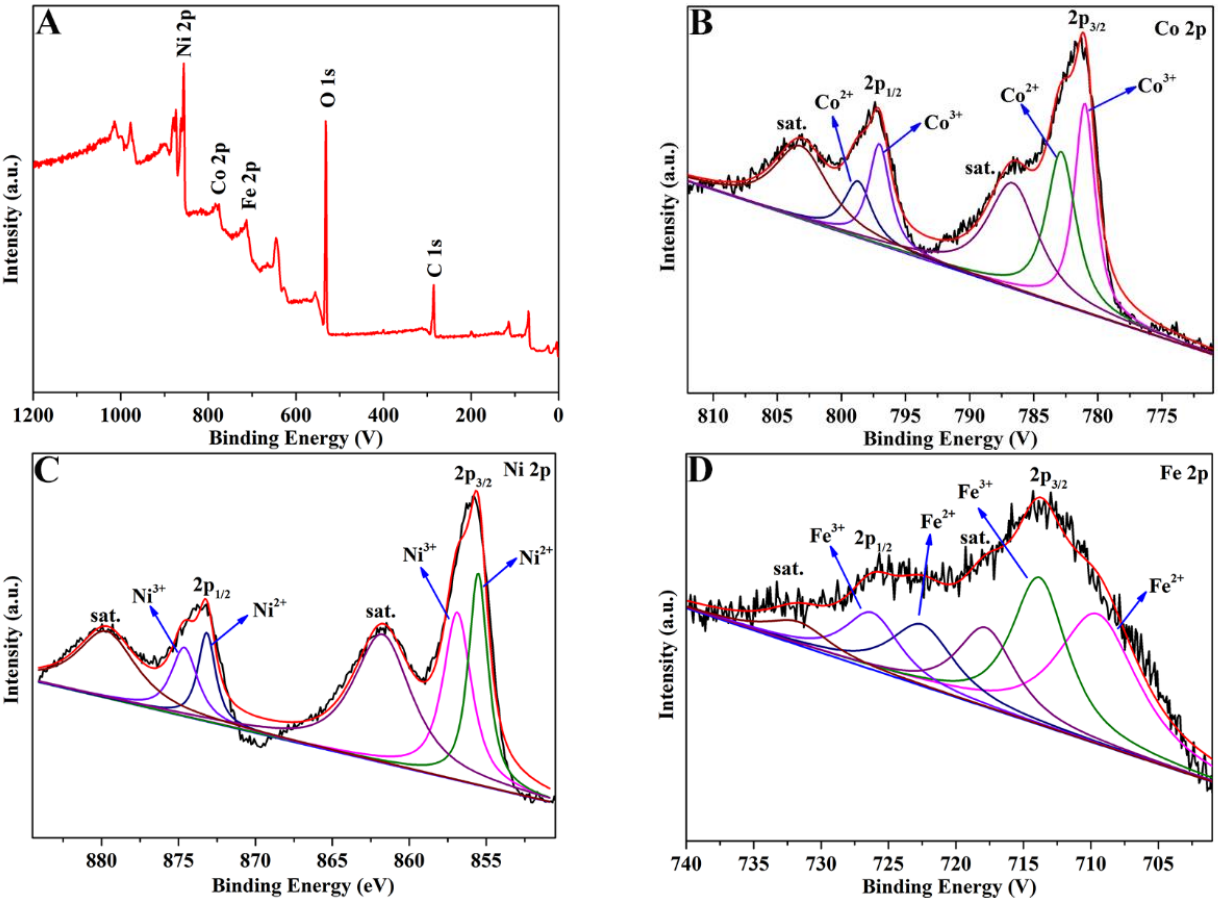

Figure 5. XPS spectra of CC@CCH NiFe LDH: (A) survey spectrum, (B) Co 2p, (C) Ni 2p and (D) Fe 2p.

As shown in Fig. 5 (A-D), the elemental composition and valence state of the elements in CC@CCH NiFe LDH were further studied by X-ray photoelectron spectroscopy (XPS). Fig. 5A shows that the XPS survey spectrum displays the coexistence of five elements C, O, Co, Ni and Fe. The XPS spectra of Co 2p, Ni 2p and Fe 2p fitted by Gaussian fitting method are shown in Fig. 5B, 5C and 5D, respectively. Due to the splitting of the spin orbit, the spectra of Co 2p, Ni 2p and Fe 2p exhibit $2p_{1/2}$ and $2p_{3/2}$ components. In the Co 2p spectrum (Fig. 5B), two main peaks can be clearly observed at 781.21 and 796.36 eV, corresponding to Co $2p_{3/2}$ and Co $2p_{1/2}$. The peaks of 781.05 and 796.26 eV are characteristic of Co^{3+} peaks, while the peaks of 782.55 and 797.63 eV are derived from Co^{2+}, illustrating the presence of both Co^{3+} and Co^{2+} valence states in CC@CCH NiFe LDH. In addition, 788.66 and 802.75 eV correspond to two satellite peaks. The peak intensity of the satellite is weak, indicating that Co exists in the form of Co^{3+} [31, 40]. As shown in Fig. 5C, in the Ni 2p spectrum, the strong peaks of 855.81 and 873.45 eV correspond to Ni $2p_{3/2}$ and Ni $2p_{1/2}$, and the two satellite peaks are located near 861.98 and 879.78 eV. Meanwhile, the binding energy at 855.51 and 873.14 eV corresponds to Ni^{2+}, and the binding energy of 856.73 and 874.71 eV corresponds to Ni^{3+}, confirming the existence of Ni^{2+} and Ni^{3+}. However, the stronger satellite peak indicates that Ni^{2+} is the predominant form of Ni [28, 31, 40]. Similarly, in Fig. 5D, the energy of the two spin-orbital dipoles

$2p_{1/2}$ and $2p_{3/2}$ of the Fe 2p spectrum are 713.58 and 724.88 eV. The satellite peaks are located at 718.08 and 731.78 eV, and the peak intensity of the satellite is extremely weak, indicating that Fe exists in the form of Fe^{3+} [28, 41, 42]. The above results further confirm the successful preparation of CC@CCH NiFe LDH.

3.2 Electrochemical performance of electrode materials

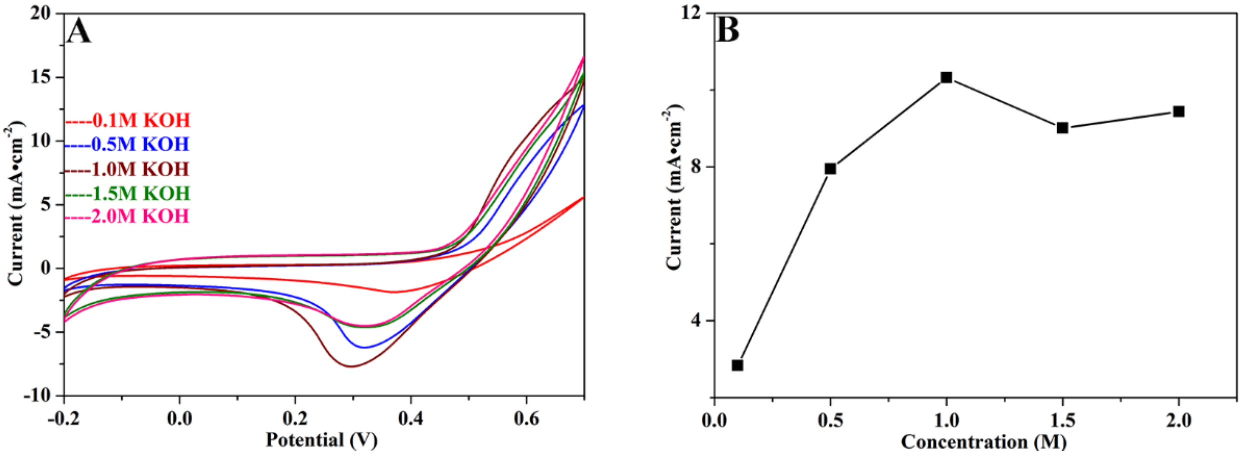

Figure 6. (A) CV curves of CC@CCH NiFe LDH with continuously add 0.5 mM glucose into different concentrations of KOH at a scan rate of 10 mV s^{-1}; (B) The corresponding plot of the anodic peak current density and KOH concentration.

The electrolyte concentration is important for the catalytic oxidation activity of non-enzymatic glucose sensors. Therefore, the effects of CC@CCH NiFe LDH electrode materials were investigated about glucose oxidation at different KOH concentrations. From Fig. 6A and 6B, it can be seen that the oxidation peak current density gradually increases as the KOH concentration increases, reaching a maximum at 1 M. Then, it decreases as the KOH concentration further increases. Therefore, 1 M KOH solution was selected as the electrolyte solution for electrochemical test.

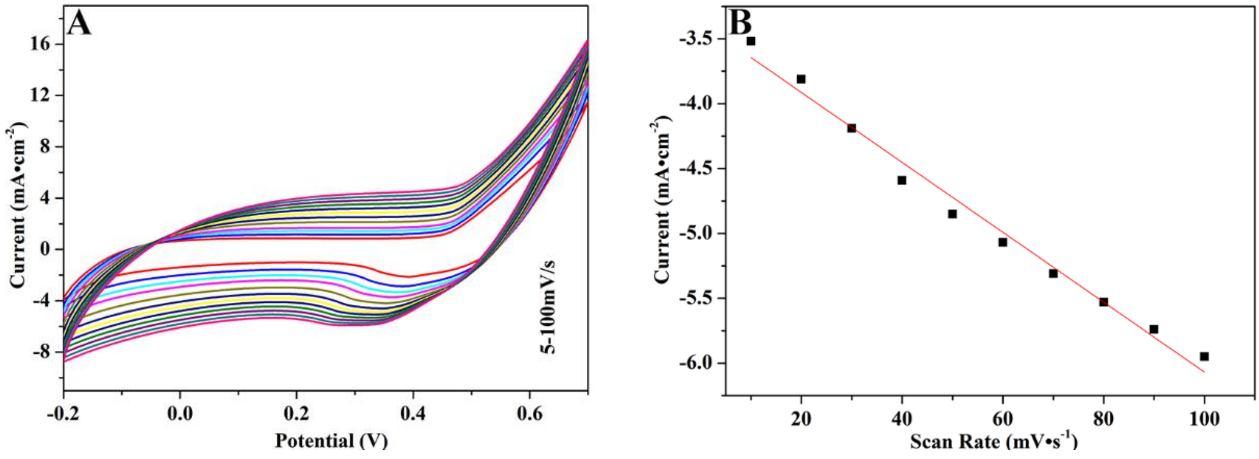

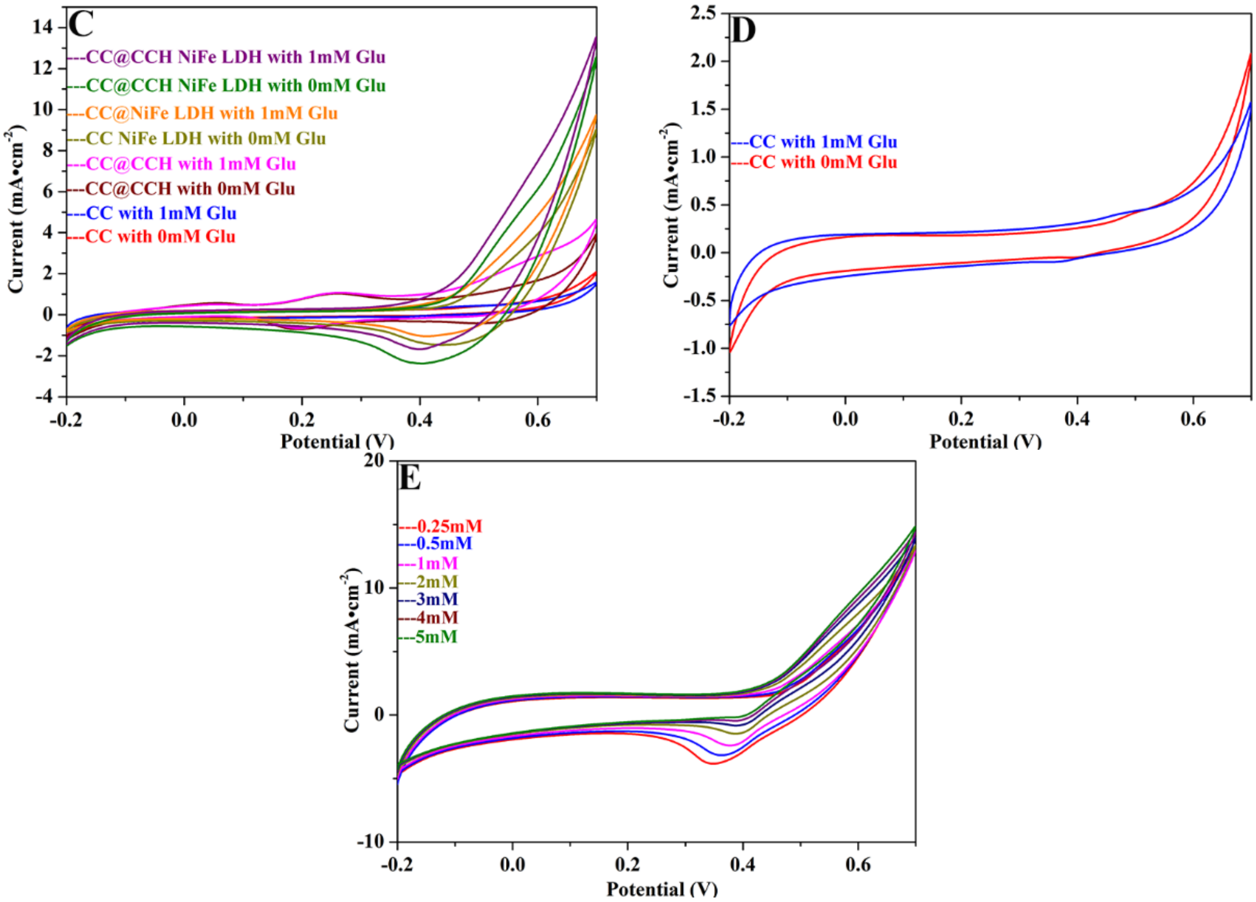

Figure 7. (A) CV curves of CC@CCH NiFe LDH in 1 M KOH with different scan rate; (B) Calibration curves for (A); (C) CV curves of different electrode composites in 1 M KOH without or with 1 mM glucose at 10 mV s^{-1}; (D) The enlarged view of CV curves of CC electrode material in 1 M KOH without or with 1 mM glucose at 10 mV s^{-1}; (E) CV curves of CC@CCH NiFe LDH in 1 M KOH with different glucose concentrations.

In order to investigate the effect of scanning rate on CC@CCH NiFe LDH electrode, cyclic voltammetry (CV) was used in 1 M KOH solution for related tests. Fig. 7A shows the CV curves of the scanning rate within the range of 5-100 mV·s^{-1} and the voltage within the range of -0.2-0.7 V. The result displays that the peak current density of CC@CCH NiFe LDH gradually increases with the increase of scanning rate. However, apparent electrochemical polarization phenomena will limit the transmission of electrons and ions at high scan rates. Fig. 7B shows the relationship between cathode peak current density and scan rate. It can be observed that the cathode peak current density is linear with the scan rate, and the correlation coefficient is 0.98374. The result indicates that ion transfer involved in the CC@CCH NiFe LDH electrode material during the redox reaction is a surface control process.

CC, CC@CCH, CC@NiFe LDH and CC@CCH NiFe LDH were studied with or without glucose in a voltage range of -0.2-0.7 V and a scan rate of 10 mV s^{-1}. Fig. 7C shows that CC@CCH, CC@NiFe LDH and CC@CCH NiFe LDH electrodes have catalytic oxidation properties for glucose, but the CV integral area of CC@CCH NiFe LDH electrodes is obviously larger than CC@CCH and CC@ NiFe. LDH, illustrating that its Faraday redox rate is faster and it has better electrochemical performance. Compared with CC@CCH and CC@NiFe LDH, the CC@CCH NiFe LDH electrode has the largest increase in redox peak current density, demonstrating the importance of hierarchical structure in improving electrocatalytic performance. In contrast, bare CC electrode has little catalytic oxidizing power for glucose (Fig. 7D), confirming that CC acts only as a conductive substrate and does not participate in the glucose oxidation process. Meanwhile, in order to further explore the electrocatalytic behavior of CC@CCH NiFe LDH on glucose oxidation, different concentrations of glucose solution were studied by CV technique. It can be observed from Fig. 7E that the oxidation current density increases with the increase of glucose concentration at 0-5 mM, and the potential also moves toward a positive potential.

Since the sensitivity of the glucose sensor is highly dependent on the working potential, the amperometric tests were performed on the CC@CCH NiFe LDH electrode over a voltage range from 0.45 to 0.70 V. And 0.1 mM glucose solution was continuously added into the 1 M KOH electrolyte. At the same time, in order to ensure the uniform distribution of glucose in the electrolytic cell, the electrolyte solution needs to be constantly stirred during the whole experiment. As shown in Fig. 8A, although the applied voltage is different, when 0.1 mM glucose solution is continuously added, the response current density shows an increasing trend, and the response current density increases as the applied potential increases, indicating that the increase of applied potential helps the improvement of current response. However, when the applied voltage is too high, the background current also increases.

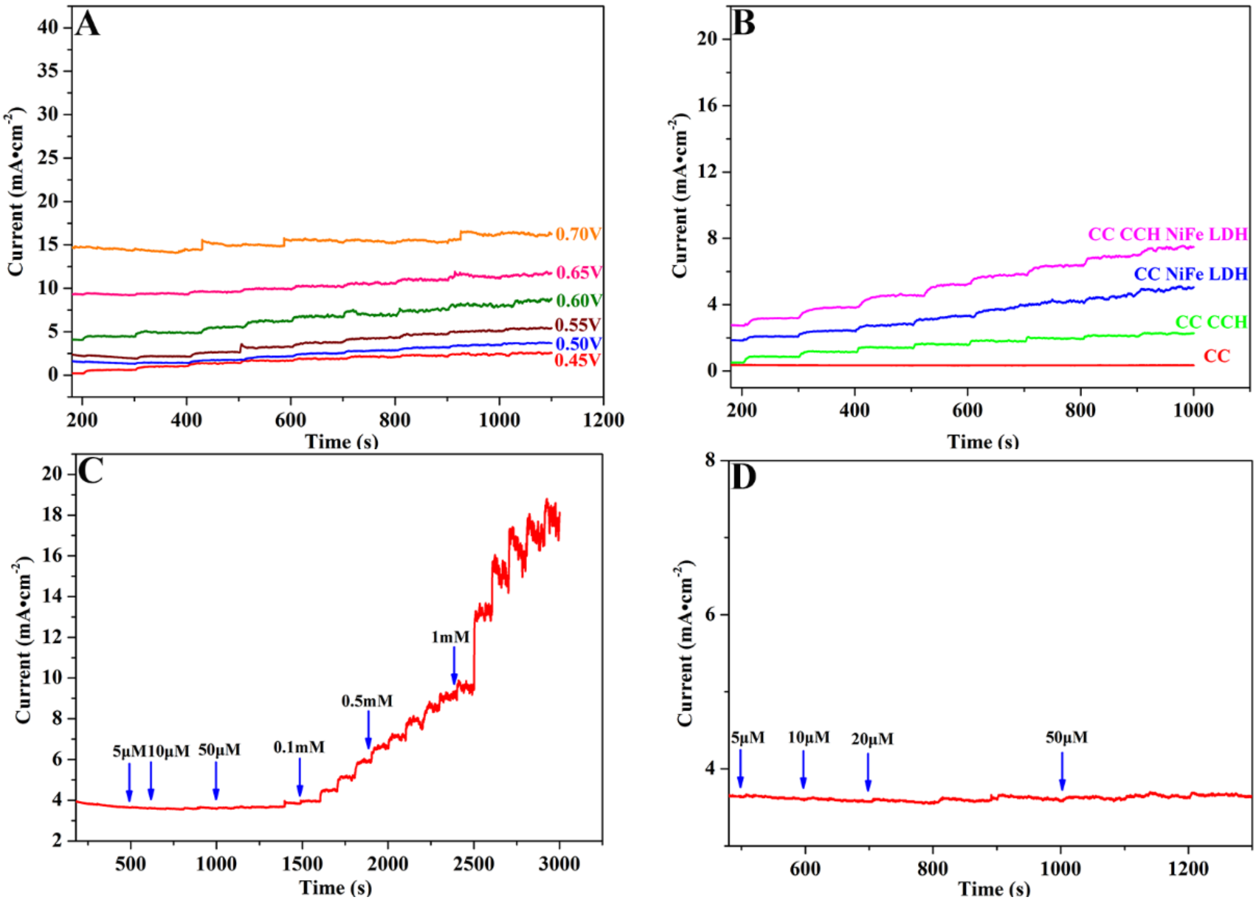

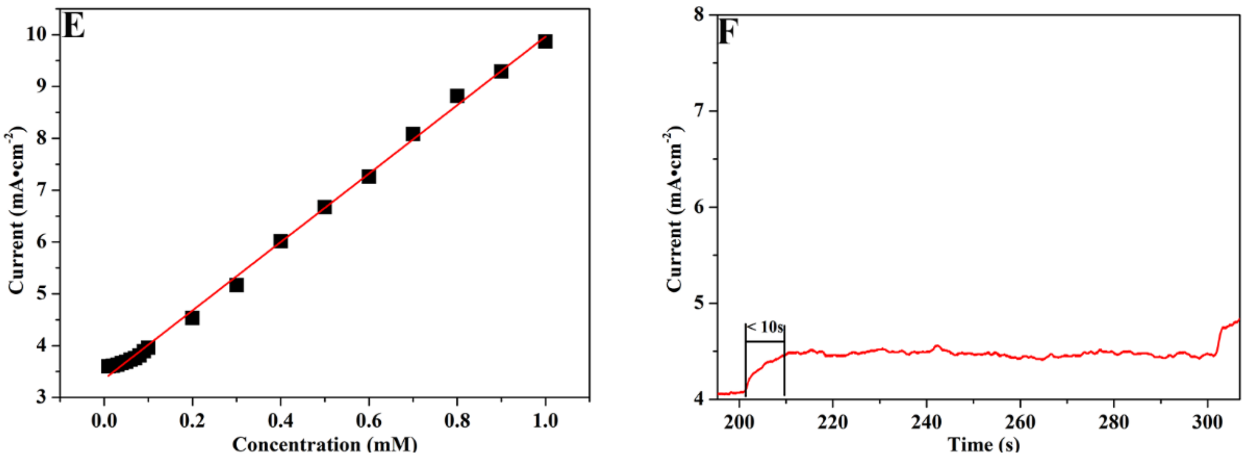

Figure 8. (A) Amperometric response of CC@CCH NiFe LDH in 1 M KOH with 0.1 mM glucose at different potentials; (B) Amperometric response curves of CC, CC@CCH, CC@NiFe LDH, CC@CCH NiFe LDH with successive addition glucose at 0.60 V in 1 M KOH; (C) Amperometric responses of CC@CCH NiFe LDH with different concentration glucose addition in 1 M KOH; (D) The amperometric responses of CC@CCH NiFe LDH in low glucose concentration; (E) Calibration curve of current response and different glucose concentration; (F) The response time of CC@CCH NiFe LDH with 0.1 mM glucose.

Therefore, 0.60 V was chosen as the optimal voltage for glucose detection. In addition, amperometric response tests were performed on CC, CC@CCH, CC@NiFe LDH, and CC@CCH NiFe LDH electrode materials at this voltage. It can be clearly seen from Fig. 8B that CC@CCH NiFe LDH has the best response performance. It is better to illustrate that the hierarchical structure of CC@CCH NiFe LDH electrode material greatly improves the electrochemical sensing performance.

Fig. 8C shows the ampere response of CC@CCH NiFe LDH electrode material after continuous addition glucose solution with different concentrations under the conditions of 0.60 V and 1 M KOH. It can be seen that the response current density increases stepwise with the continuous addition glucose, and the response speed is faster, reaching the steady state value within 10 s (Fig. 8F). Fig. 8D displays that the stepwise increases trend of the current response curve of CC@CCH NiFe LDH can be clearly observed even at low glucose concentration. Furthermore, the response current density of the CC@CCH NiFe LDH electrode shows a good linear relationship with the glucose concentration (Fig. 8E). The fitting curve equation was as follows: j (mA·cm^{-2}) = 6.61 c (mM) + 3.35, and the correlation coefficient is 0.9997. The detection range is from 10 μM to 1 mM, and the detection sensitivity of the sensor is 6610 μA·mM^{-1}·cm^{-2}. In addition, the minimum detection limit is calculated to be 3 μM (S/N=3). The above results show that the CC@CCH NiFe LDH electrode exhibits excellent electrochemical performance as a non-enzymatic glucose sensing platform. This is attributed to the following advantages: (i) a stable structure was obtained by in situ growth; (ii) the rod structure of CCH and the layered crystal structure of LDH promote the transport of ions and electrons in the active material; (iii) the 3D hierarchical structure of the CC@CCH NiFe LDH electrode provides more active sites for electrocatalytic detection. Compared with the previous non-enzymatic glucose sensors, CC@CCH NiFe LDH exhibits excellent electrochemical performance in sensitivity and selectivity, as shown in Table 1.

Table 1. Performance comparisons of CC@CCH NiFe LDH electrode with other non-enzymatic glucose biosensors.

Electrodes	Sensitivity($\mu A \cdot mM^{-1} \cdot cm^{-2}$)	Linear range (mM)	LOD (μM)	Ref.
CC@CCH NiFe LDH	6610	0.01-1	3	This work
CuNPs/rGO	447.65	0.01-1.2	3.4	[43]
$CuNiCoO_4$ NWs@CC	1782	0.02-1.4	6.5	[33]
CNFS/$Co(OH)_2$	6800	0.01-0.12	5	[44]
Co_3O_4 nanooctahedrons	248.6	0.5-1.0	0.012	[5]
Ni(II)-CP/C_{60}/GCE	614	0.01-3	4.3	[16]
Co_3O_4-GR	~	0.05-0.3	10	[45]
Defect-rich $Ni(OH)_2$/NiO nanosheet	2931	0.09-1.08	5.0	[46]
α-$Ni(OH)_2$/FTO	446	~ 0.75	3	[47]

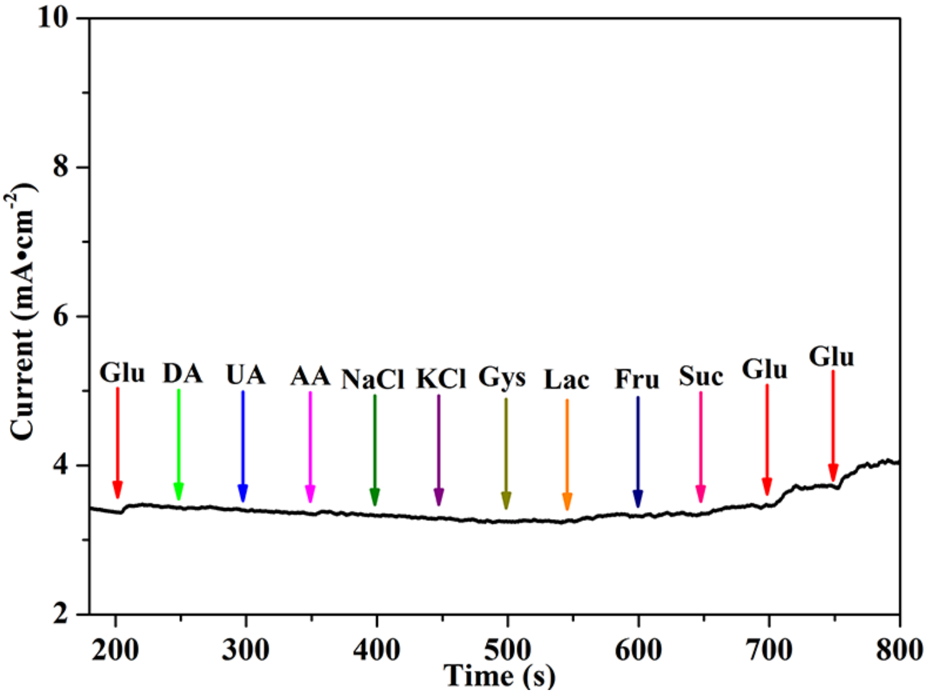

Figure 9. Amperometric responses of CC@CCH NiFe LDH upon the addition of various interferences in 1 M KOH.

In addition, selectivity is another important parameter for analyzing non-enzymatic electrochemical sensors. In general, organic and inorganic reagents (such as dopamine, uric acid, chloride ions) coexist with glucose in the blood, which is interfering with glucose detection [3, 5, 8, 15]. Therefore, in assessing the sensitivity and selectivity of electrode materials for glucose detection, it is critical to eliminate these interfering factors. Generally, the glucose concentration in the normal physiological level of the human body is more than ten times that of the above interfering substances. In this work, the ampere response of the CC@CCH NiFe LDH electrode was detected by adding 0.1 mM glucose and 0.02 mM interfering substances, respectively. Fig. 9 shows the ampere response curves after addition of 0.1 mM glucose, 0.02 mM uric acid (UA), potassium chloride (KCl), dopamine (DA),cysteine (Cys), lactose (Lac), ascorbic acid AA), fructose (Fru), ucrose (Suc) and sodium chloride (NaCl) at 0.60 V. From this curve, it can be clearly seen that the CC@CCH NiFe LDH electrode has an obvious current response when 0.1 mM glucose is added, while the current response does not change significantly or even no respond when interfering substances are added. When 0.1 mM glucose solution was added again, the current density increased immediately. The results show that the electrode has good selectivity for glucose detection.

4. CONCLUSION

In summary, a binder free 3D hierarchical nanomaterial sensor (CC@CCH NiFe LDH) was successfully prepared on CC by a simple hydrothermal method. This novel hierarchical layered material has the following advantages: (i) the CCH-NiFe LDH deposited on the CC can be used directly as an electrode, avoiding the use of polymer binder and conductive agent; (ii) pre-grown 1D CCH nanorods arrays provide more active sites as support for 2D NiFe LDH nanosheets; (iii) the CC@CCH NiFe LDH electrode material has excellent electrocatalytic oxidation activity. The researches show that the excellent catalytic oxidation performance of the electrode material includes high sensitivity, wide detection range, low detection limit and good selectivity for high concentration interferences. The above results show that the electrode material of 3D hierarchical structure developed in this paper is expected to achieve accurate detection of glucose in biotechnology.

ACKNOWLEDGEMENTS

This research was supported by the National Natural Science Foundation of China (No.51908408) and the Science & Technology Development Fund of Tianjin Education Commission for Higher Education (2018KJ202).

References

1. E. Asadian, S. Shahrokhian and A.I. Zad, *J. Electroanal. Chem.*, 808 (2018) 114.
2. S. Fu, G. Fan, L. Yang and F. Li, *Electrochim. Acta*, 152 (2015) 146.
3. Y. Li, M. Xie, X. Zhang, Q. Liu, D. Lin, C. Xu, F. Xie and X. Sun, *Sens. Actuators B*, 278 (2019) 126.
4. S. Felix, A.N. Grace and R. Jayavel, *J. Phys. Chem. Solids*, 122 (2018) 255.
5. J. Xu, F. Li, D. Wang, M.H. Nawaz, Q. An, D. Han and L. Niu, *Biosens. Bioelectron.*, 123 (2019) 25.
6. B. Xue, K. Li, L. Feng, J. Lu and L. Zhang, *Electrochim. Acta*, 239 (2017) 36.

7. J. Zhou, M. Min, Y. Liu, J. Tang and W. Tang, *Sens. Actuators B*, 260 (2018) 408.
8. F. Liu, P. Wang, Q. Zhang, Z. Wang, Y. Liu, Z. Zheng, X. Qin, X. Zhang, Y. Dai, L. Li and B. Huang, *Anal. Bioanal. Chem.*, 410 (2018) 7663.
9. T. Chen, D. Liu, W. Lu, K. Wang, G. Du, A.M. Asiri and X. Sun, *Anal. Chem.*, 88 (2016) 7885.
10. B. Hai and Y. Zou, *Sens. Actuators B*, 208 (2015) 143.
11. F. Wang, Y. Zhang, W. Liang, L. Chen, Y. Li and X. He, *Sens. Actuators B*, 273 (2018) 41.
12. W. Lu and X. Wu, *New J. Chem.*, 42 (2018) 3180.
13. J. Chen, Q. Sheng, Y. Wang and J. Zheng, *Electroanalysis*, 28 (2016) 979.
14. D. Jiang, Z. Chu, J. Peng, J. Luo, Y. Mao, P. Yang and W. Jin, *Electrochim. Acta*, 270 (2018) 147.
15. G. Ni, J. Cheng, X. Dai, Z. Guo, X. Ling, T. Yu and Z. Sun, *Electroanalysis*, 30 (2018) 2366.
16. L. Shahhoseini, R. Mohammadi, B. Ghanbari and S. Shahrokhian, *Appl. Surf. Sci.*, 478 (2019) 361.
17. G. Yilmaz, K.M. Yam, C. Zhang, H.J. Fan and G.W. Ho, *Adv. Mater.*, 29 (2017).
18. T. Zhan, J. Kang, X. Li, L. Pan, G. Li and W. Hou, *Sens. Actuators B*, 255 (2018) 2635.
19. M, Zhang, Z. Luo, M. Zhou, G. Zhang, K.A. Alamry, L.A. Taib, A.M .Asiri and X. Wang, *Appl. Catal., B*, 210 (2017) 454.
20. H. Zhang, X. Li, A. Hähnel, V. Naumann, C. Lin, S. Azimi, S.L. Schweizer, A.W. Maijenburg and R.B. Wehrspohn, *Adv. Funct. Mater.*, 28 (2018).
21. J. Xie, W. Chen, X. Wu, Y. Wu and H. Lin, *Anal. Methods*, 9(2017) 974.
22. Y. Zhang, J. Tian, S. Liu, L. Wang, X. Qin, W. Lu, G. Chang, Y. Luo, A.M. Asiri, A.O. Al-Youbi and X. Sun, *Analyst*, 137(2012) 1325.
23. Z. Jiang, Z. Li, Z. Qin, H. Sun, X. Jiao and D. Chen, *Nanoscale*, 5 (2013) 11770.
24. S. Li, L. Wang, Y. Li, L. Zhang, A. Wang, N. Xiao, Y. Gao, N. Li, W. Song, L. Ge and J. Liu, *Appl. Catal., B*, 254 (2019) 145.
25. W. Chen, J. Wang, K.Y. Ma, M. Li, S.H. Guo, F. Liu and J.P. Cheng, *Appl. Surf. Sci.*, 451 (2018) 280.
26. Z. Deng, Y. Sun, Y. Wang and J. Gao, *Sensors*, 18(2018) .
27. Y. Tao, Q. Chang, Q. Liu, G. Yang, H. Guan, G. Chen and C. Dong, *Surf. Interface Anal.*, 12 (2018) 102.
28. H. Xu, B. Wang, C. Shan, P. Xi, W. Liu and Y. Tang, *ACS Appl. Mater. Interfaces*, 10 (2018) 6336.
29. H. Chen, L. Hu, M. Chen, Y. Yan and L. Wu, *Adv. Funct. Mater.*, 24 (2014) 934.
30. M. Huang, D. He, M. Wang and P. Jiang, *Anal. Bioanal. Chem.*, 410 (2018) 7921.
31. H. Liang, J. Lin, H. Jia, S. Chen, J. Qi, J. Cao, T. Lin, W. Fei and J. Feng, *J. Power Sources*, 378 (2018) 248.
32. J. Ma, J. Li, R. Guo, H. Xu, F. Shi, L. Dang, Z. Liu, J. Sun and Z. Lei, *J. Power Sources*, 428 (2019) 124.
33. H. Mirzaei, A.A. Nasiri, R. Mohamadee, H. Yaghoobi, M. Khatami, O. Azizi, M.A. Zaimy and H. Aziziz, *Microchem. J.*, 142 (2018) 343.
34. X. Wang, Y. Zheng, J. Yuan, J. Shen, J. Hu, A. Wang, L. Wu and L. Niu, *Electrochim. Acta*, 224 (2017) 628.
35. F. Xin, Y. Jia, J. Sun, L. Dang, Z. Liu and Z. Lei, *ACS Appl. Mater. Interfaces*, 10(2018) 32192.
36. L. Zhi, W. Zhang, L. Dang, J. Sun, F. Shi, H. Xu, Z. Liu, Z. Lei, *J. Power Sources*, 387 (2018) 108.
37. Y. Wang, W. Ding, S. Chen, Y. Nie, K. Xiong and Z. Wei, *Chem. Commun.*, 50 (2014) 15529.
38. J. Zhou, Y. Dou, A. Zhou, R. Guo, M. Zhao and J. Li, *Adv. Energy Mater.*, 7 (2017).
39. N. Nesakumar, S. Anantharaj, N. Subramanian, S. Kundu and S. Alwarappan, *J. Electrochem. Soc.*, 165 (2018) B536.
40. D. Zha, Y. Fu, L. Zhang, J. Zhu and X. Wang, *J. Power Sources*, 378 (2018) 31.
41. W. Liu, X. Hu, H. Li and H. Yu, *Small*, 14 (2018).
42. L. Yang, G. Zhu, H. Wen, X. Guan, X. Sun, H. Feng, W. Tian, D. Zheng, X. Cheng and Y, Yao, *J Mater. Chem. A*, 7 (2018) 8771.
43. Q. Wang, Q. Wang, M. Li, S. Szunerits and R. Boukherroub, *RSC Adv.*, 5(2015) 15861.

44. Q. Wang, Y. Ma, X. Jiang, N. Yang, Y. Coffinier, H. Belkhalfa, N. Dokhane, M. Li, R. Boukherroub and S. Szunerits, *Electroanalysis*, 28 (2015) 119.
45. X. Wang, X. Dong, Y. Wen, C. Li, Q. Xiong and P. Chen, *Chem. Commun.*, 48 (2012) 6490.
46. W. Huang, L. Ge, Y. Chen, X. Lai, J. Peng, J. Tu, Y. Cao and X. Li, *Sens. Actuators B*, 248 (2012) 169.
47. P.R. Martins, M.A. Rocha, L. Angnes, H.E. Toma and K. Araki, *Electroanalysis*, 23 (2011) 2541.